Stability of Haptic Displays

D. W. Weir and J. E. Colgate

This chapter reviews the issue of instability in haptic devices, as well as the related concept of Z-width. Methods for improving haptic display performance (expanding the Z-width) are also discussed.

8.1 Definitions

Haptic displays can be considered to be devices which generate mechanical impedances. 'Impedance' here is defined as a dynamic relationship between velocity and force. The behavior of the haptic display depends on the virtual environment being rendered. For instance, if the desired behavior is that of a point mass, the haptic display must exert forces proportional to acceleration. Similarly, if the desired behavior is that of a spring, the haptic display must exert forces proportional to displacement [Colgate and Brown 94].

Passivity has proved to be a useful tool for studying both the stability and performance of haptic displays. A one-port system is passive if the integral of the power extracted over time does not exceed the initial energy stored in the system. For a translational mechanical system, power is the product of force (f) and velocity ($\dot{x}$), with the sign convention that power is positive when energy flows into the system. Typically, the initial energy is defined to be zero, resulting in the following inequality:

$$\int_0^t f(\tau)\dot{x}(\tau)d\tau \geq 0, \qquad \forall t \geq 0 \tag{8.1}$$

A passive system, coupled with any other passive system, is necessarily stable. Ordinary physical objects, such as springs, masses, and dampers, are passive, and common experience suggests that humans remain stable when interacting with passive systems. Therefore, the human user is typically considered a passive impedance, particularly at high frequencies above the bandwidth of voluntary motion. If a haptic display rendering an arbitrary virtual environment can be guaranteed passive, then the complete system will be stable when the display is coupled with the human operator. This property frees the designer from having to analyze the interaction of

the haptic display and virtual environment with the human operator under all possible configurations.

In the real world, objects interact according to a set of physical laws that govern their behavior. In the virtual world, this interaction is only approximated. Even though the approximate behavior may be very close to the real behavior, the implications of these errors can be profound. Instability and limit cycle oscillations are two common ways in which haptic interactions deviate from their physical counterparts, both of which result from non-passivity. Small amplitude limit cycle oscillations can be particularly problematic even if they do not escalate to gross instability because human tactile perception is extremely sensitive to vibrations in the 100Hz to 1kHz range [Bolanowski et al. 88]. Maintaining passivity is one way, albeit sometimes restrictive, of ensuring that virtual objects behave in a stable manner when interacting.

Everyday interaction with common objects involves experiencing a wide range of impedances. Moving in free space implies almost zero resistance to motion, while interacting with tables, walls, and other massive objects provide almost complete resistance to motion. The challenge is to design a haptic interface that can display as wide a range of dynamic impedances as possible.

The dynamic range of impedances that can be rendered by a haptic display while maintaining passivity is termed its Z-width. Since a display with larger Z-width will usually render "better" feeling virtual environments, Z-width may be viewed as a measure of quality for the haptic display.

As a final note, we should mention that haptic displays are often referred to as "impedance type" or "admittance type." Impedance displays measure the endpoint motion and output a force or torque in response. Admittance displays measure the applied force or torque and output a motion. Both systems respond according to the (imperfectly) simulated physics of the virtual environment being rendered. This chapter will address both impedance and admittance displays, but will focus primarily on impedance causality displays. Note, however, that for either type, the notions of passivity and Z-width are equally valid.

8.2 Designing for Passivity

Expanding the impedance range of a haptic display as a method for improving performance begins with passivity. Maintaining passivity places severe restrictions on virtual environment stiffness and damping; therefore, a number of techniques have been developed to facilitate haptic rendering of high impedance environments.

Due to the nature of impedance causality haptic displays, the lower

bound on impedance is generally limited by the quality of force sensing and feedback, and the mechanical design. Often, impedance causality displays feature low inertia designs enabling low impedance renderings. The upper bound on passive impedance can be limited by sensor quantization, sampled data effects, time delay, and noise [Colgate and Schenkel 97]. Thus, most research efforts have focused on increasing the maximum impedance that can be displayed as a way of increasing the Z-width of haptic displays.

A number of methods exist to increase the maximum passive impedance of a haptic interface. These fall into a number of broad categories: controllers, physical mechanisms, and electrical mechanisms. The category of controllers includes virtual couplings and passivity observers. Virtual couplings act as mediators between the haptic display and the virtual environment. Passivity observers and passivity controllers function by adjusting the energy present in the system to maintain passivity. Mechanical methods are generally the most direct, whereby physical dissipation is added to the mechanism to expand the passive impedance range of a haptic display by counteracting the effects of energy leaks. Electrical methods are a blend of physical methods implemented electrically and controller approaches implemented using analog electronics.

In a slightly different category are psychophysical techniques that act to alter the user's perception of the impedance range of the haptic display. These include methods such as rate hardness and event-based rendering.

8.3 Passive Rendering of a Virtual Wall

8.3.1 A Simple Passivity Result

Haptic displays are sampled-data systems, i.e., they combine a continuous-time mechanical system with a discrete-time controller. The effects of sampling, even assuming ideal sensors and actuators in the continuous-time plant, cause a haptic display to lose passivity.

[Colgate and Schenkel 97] derive an analytical passivity criterion for a simple 1 degree of freedom (DOF) haptic interface, as shown in Figure 8.1. The discrete-time controller models a virtual wall, including a unilateral constraint operator and includes analog-to-digital (A/D) and digital-to-analog (D/A) converters in the feedback loop. A block diagram for this sampled-data system is shown in Figure 8.2. The unilateral constraint is chosen as a fundamental building block for virtual environments, because it models a simple form of contact and collision between two objects.

A necessary and sufficient condition for passivity of the sampled data system in Figure 8.1 is:

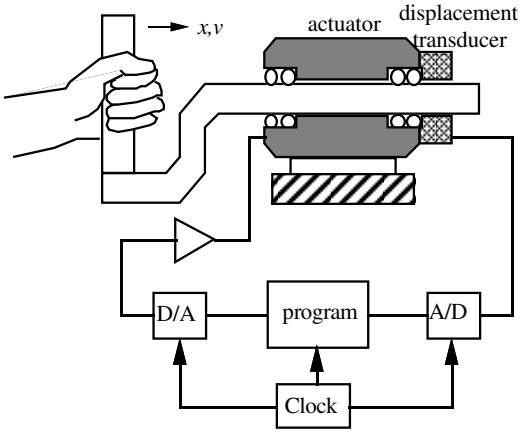

Figure 8.1: A simple 1 DOF haptic display [Colgate and Schenkel 97].

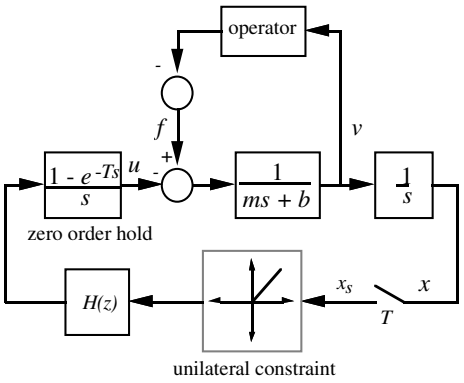

Figure 8.2: Block diagram of a haptic display and operator sampled-data system [Colgate and Schenkel 97].

$$b > \frac{T}{2}\frac{1}{1-\cos(\omega T)}\Re\{(1-e^{-j\omega T})H(e^{j\omega T})\} \qquad \text{for} \quad 0 \leq \omega \leq \omega_N \tag{8.2}$$

where b is the physical damping present in the mechanism, T is the sampling rate, $H(z)$ is a pulse transfer function representing the virtual environment, and $\omega_N = \frac{\pi}{T}$ is the Nyquist frequency [Colgate and Schenkel 97].

The result can be simplified to an analytical expression relating the

sampling rate, virtual stiffness, virtual damping, and dissipation within the haptic display. [Colgate and Schenkel 97] analyze a wall consisting of a virtual spring and damper in mechanical parallel, together with a unilateral constraint operator. A velocity estimate is obtained from backward difference differentiation of the position sensor data. This results in the following transfer function within the wall:

$$H(z) = K + B\frac{z-1}{Tz} \tag{8.3}$$

where $K > 0$ is the virtual stiffness and B is the virtual damping coefficient (B is allowed to be positive or negative). Equation 8.2 combined with Equation 8.3 simplifies to the following passivity condition:

[Colgate and Schenkel 97]

$$b > \frac{KT}{2} + |B| \tag{8.4}$$

The physical damping present in the mechanism must be sufficient to dissipate the excess energy created by errors introduced by sampling in the discrete-time controller, commonly referred to as "energy leaks."

8.3.2 Importance of Damping

The physical damping present in the haptic display is critically important, due to its role in counteracting the energy generation from errors introduced by sensing and discrete-time control. [Colgate et al. 93] expand on the passivity bound of Equation 8.4 and provide simulation data showing how maximizing sensor resolution and minimizing sampling rate improves performance. Colgate and co-authors also introduce the concept of adding physical damping to the system in order to increase the limits of virtual stiffness and virtual damping that can be passively achieved [Colgate et al. 93, Colgate and Schenkel 97, Colgate and Brown 94].

The implications of Equation 8.4 are somewhat counterintuitive: to increase the maximum impedance of a haptic display, increase the viscous damping in the mechanism in order to maintain passivity. The addition of physical damping can dramatically increase the maximum passive impedance a device can render. When low impedances are rendered, virtual damping in the discrete-time controller can be negative, masking the increased physical damping in the device. However, simulated or virtual damping cannot substitute for real, physical dissipation in the mechanism [Colgate and Brown 94]. Physical damping can be added to the haptic interface through a variety of techniques that will be discussed in Part II.

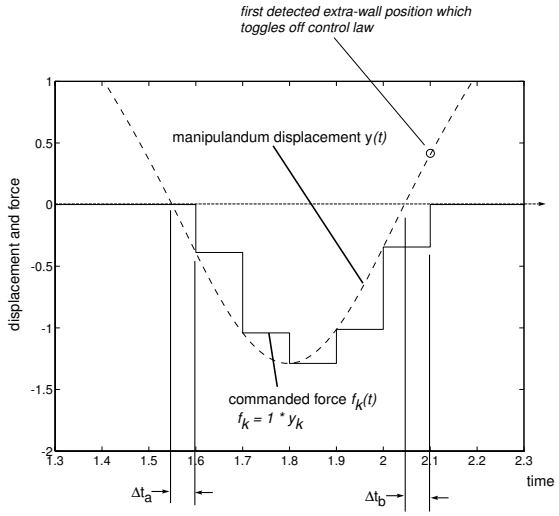

Figure 8.3: The effect of sampling: actual position, sampled position, commanded force [Gillespie and Cutkosky 96].

8.3.3 Virtual Wall as a Benchmark

The virtual wall is the standard haptic task. Since most interaction with virtual environments can be simplified to interaction with a virtual wall of varying stiffness and damping, the virtual wall is commonly used as a performance benchmark for haptic interfaces. For example, see [Colgate and Brown 94], [Gillespie and Cutkosky 96], [Zilles and Salisbury 95], [Adams and Hannaford 99], and [Abbott and Okamura 05].

Due to the nature of sampling, simulating the behavior of a stiff virtual wall is a difficult task. To characterize the general problem, consider the following example. As a general rule, there is always some penetration of the position of the haptic display into the virtual wall. As a consequence, at the next sampling interval, the discrete controller detects the wall penetration, and the virtual environment computes large output forces normal to the wall surface. This large force has a tendency to rapidly push the haptic display outside of the virtual wall into free space. This situation now reverses, where at some future sampling interval, the position of the haptic display is outside the virtual wall, so the forces return to zero. This sequence is depicted in Figure 8.3. Oscillations arise when this cycle of free space and wall penetration is repeated. Sampling prevents detecting the exact time when the haptic display contacts the surface of the virtual wall, and position sensing resolution has the effect of quantizing penetra-

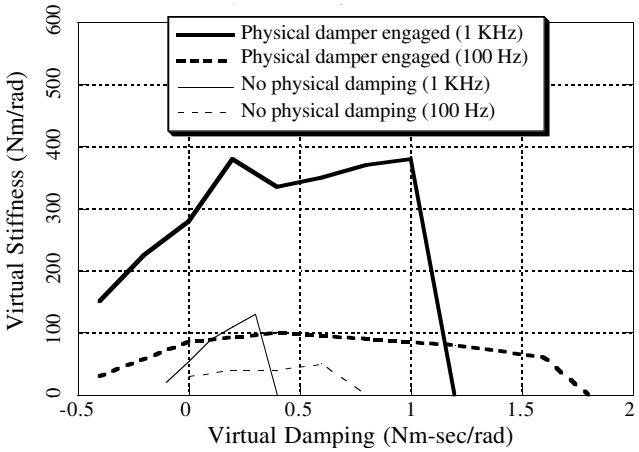

Figure 8.4: Typical Z-width plot illustrating maximum passive impedance range [Colgate and Brown 94]. (© 1994 IEEE)

tion distance into the virtual wall, both of which are destabilizing effects. These errors can lead to energy generation and active, non-passive behavior. These effects will be further addressed in in the next section.

The virtual wall is also traditionally used to characterize the impedance range, or Z-width of haptic interfaces. Z-width is often displayed using virtual stiffness-virtual damping plots, showing the maximum passive impedance boundary as the stiffness and damping vary, typically under a variety of conditions, as shown in Figure 8.4.

However this method does not show how the Z-width varies according to frequency. It also does not show the minimum stable impedance that can be rendered. The importance of this is illustrated in the following example. If a single haptic display has maximum and minimum impedances of Z_{min} and Z_{max}, respectively, then two of them in mechanical parallel will have a maximum impedance of $2Z_{max}$, increasing the boundary on the K-B plot. The minimum impedance is also increased to $2Z_{min}$, so the system Z-width has not changed, but this is not apparent on the K-B plot. This lack of minimum impedance information makes it difficult to compare various haptic interfaces.

For these reasons, a more useful figure of merit and way of displaying Z-width information may be a set of curves, showing the extremes of both impedance and admittance as a function of frequency while maintaining passivity.

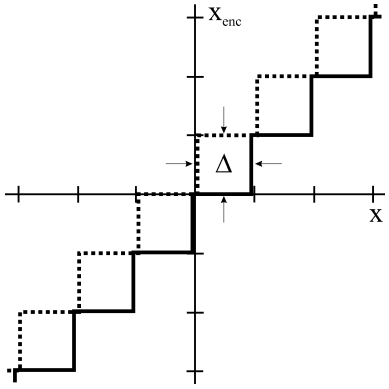

Figure 8.5: Mapping between actual position and quantized position, with sensor resolution Δ [Abbott and Okamura 05]. (© 2005 IEEE)

8.4 Extensions to the Passivity Framework

8.4.1 Quantization and Time Delay

The most common position-sensing technique for haptic displays is the use of optical encoders. One consequence of optical encoders is that position information is quantized based on the encoder resolution. Other position-sensing techniques are also frequently quantized, such as analog potentiometers that are sampled by a finite resolution analog-to-digital converter. Such a position signal would also be subject to electrical noise, but that will be not be addressed here. The distinction between sampling and sensor quantization should be emphasized. Sampling introduces uncertainty with respect to when events occur and what happens between sampling intervals. Sensor quantization causes a loss of information due to sensing only discrete changes in the value of a signal, as indicated in Figure 8.5. The actual position can lie anywhere between two quantized position measurements. Sensor quantization is independent of the sampling frequency.

In [Abbott and Okamura 05], position quantization and Coulomb-plus-viscous friction in the haptic device are explicitly modeled, as shown in Figures 8.3, 8.5, and 8.6. Analyzing the worst-case scenarios of compressing and extending a virtual spring, representing the virtual wall with a haptic display, results in this passivity condition:

$$K \leq \min\left(\frac{2b}{T}, \frac{2f_c}{\Delta}\right) \tag{8.5}$$

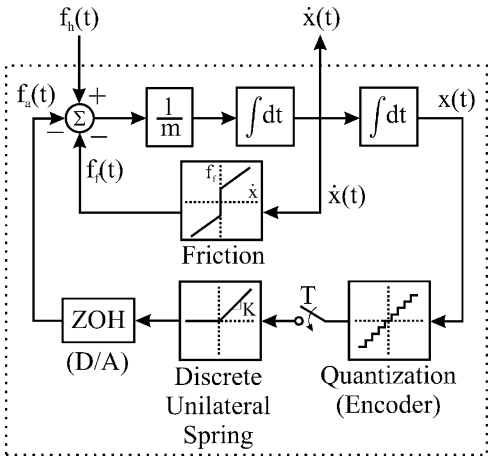

Figure 8.6: Model of haptic device rendering a virtual wall used by [Abbott and Okamura 05]. (© 2005 IEEE)

where b is the viscous damping in the mechanism, T is the sampling time, Δ is the position quantization interval, and f_c is the Coulomb friction. The haptic display is assumed to consist of a mass plus friction, and the virtual wall consists of a unilateral constraint. The first part of the inequality, $\frac{2b}{T}$, is the same as Equation 8.4 when the virtual damping is equal to zero. The stiffness is limited by the physical damping in the system, which must be sufficient to dissipate at least as much energy as the energy leaks introduced by sampling. The second term of the inequality, $\frac{2f_c}{\Delta}$, relates the Coulomb friction in the device to the encoder resolution. It should be noted that normally one of the terms is the dominating effect and provides the limiting factor for passive virtual stiffness. In the experimental verification of this passivity condition presented by [Abbott and Okamura 05], the maximum virtual stiffness limited by damping and sampling rate, $\frac{2b}{T}$, is almost two orders of magnitude smaller than the Coulomb friction limited virtual stiffness, $\frac{2f_c}{\Delta}$.

Consider the following simplified conceptual derivation of the passivity criterion in Equation 8.5 to provide an intuitive understanding of the passivity limit of virtual stiffness. Imagine compressing an ideal spring with constitutive law $F = kx$. The energy stored in the ideal spring after compressing a distance $\Delta x = x_{k+1} - x_k = vT$ during one sampling period is:

$$E = \frac{1}{2}k\Delta x^2 \tag{8.6}$$

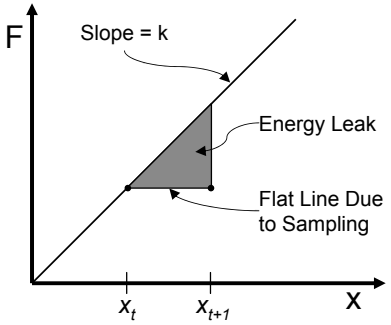

Figure 8.7: Detail of energy leak due to sampling.

Due to sampling, the force of the virtual spring remains constant between sampling intervals, as shown in Figure 8.7. Equation 8.7 is the resulting energy leak due to sampling, while at the same time, Equation 8.8 is the energy dissipated by viscous damping (assuming constant intersample velocity). In order to maintain passivity, the energy dissipated must be greater than the energy introduced by the energy leak (Equation 8.9); therefore, it is possible to calculate the maximum passive virtual stiffness, given the sampling rate and the physical dissipation (damping) in the mechanical system (Equation 8.11).

$$E_{leak} = \frac{1}{2}K(vT)^2 \tag{8.7}$$

$$E_{dissip} = bv^2T \tag{8.8}$$

$$E_{leak} \leq E_{dissip} \tag{8.9}$$

$$\frac{1}{2}Kv^2T^2 \leq Tbv^2 \tag{8.10}$$

$$K \leq \frac{2b}{T} \tag{8.11}$$

A similar derivation can be made for the virtual stiffness limit due to friction and quantization interval. Continuing with the conceptual example of rendering an ideal spring, the position of the haptic display can change to a distance equal to the quantization interval, Δ, without being sensed. This would introduce an energy leak equal to the compression of the ideal spring by a distance Δ (see Equation 8.12). The friction in the mechanism must dissipate at least as much energy as that introduced by the energy leak, which is the work done by the friction force (Equation 8.13). This inequality leads to a maximum passive virtual stiffness given the position

sensing quantization and the friction in the mechanism (Equation 8.16).

$$E_{leak} = \frac{1}{2}K\Delta^2 \tag{8.12}$$
$$E_{dissip} = f_c\Delta \tag{8.13}$$
$$E_{leak} \leq E_{dissip} \tag{8.14}$$
$$\frac{1}{2}K\Delta^2 \leq f_c(\frac{\Delta}{T})T \tag{8.15}$$
$$K \leq \frac{2f_c}{\Delta} \tag{8.16}$$

Equation 8.5 can be nondimensionalized by dividing by $2K$. The two resulting terms, β and σ, are used as axes to define a nondimensional plane depicting stability regions according to behavior, shown in Figure 8.8. This is a graphical way of depicting Equation 8.5. [Diolaiti et al. 06] analyze a similar system with the added inclusion of time delay and introduce a new nondimensionalized velocity parameter, $\dot{\xi}$.

$$\beta := \frac{b}{KT} \tag{8.17}$$
$$\sigma := \frac{f_c}{K\Delta} \tag{8.18}$$
$$position \quad \xi := \frac{x}{\Delta} \tag{8.19}$$
$$time \quad \tau := \frac{t}{T} \tag{8.20}$$
$$velocity \quad \dot{\xi}(\tau) = \frac{\dot{x}T}{\Delta} \tag{8.21}$$

One advantage of this plot is the identification of varying types of instability between regions of the plane. $\dot{\xi}$ defines a new type of behavior: it is the maximum allowed velocity of the haptic display, faster than which the small effect of Coulombic friction and virtual environment parameters can cause instability. The stability boundaries at $\beta = \sigma = \frac{1}{2}$ correspond to the effective dissipation limits for ensuring passivity, with β representing the effective limit for viscous dissipation and σ corresponding to the effective limit for Coulombic dissipation.

Quantization also limits performance through velocity estimation. Consider, for example, a slowly changing position signal with a very fast sampling rate. The finite difference method for estimating velocity is:

$$\hat{v}_k = \frac{y_k - y_{k-1}}{T} \tag{8.22}$$

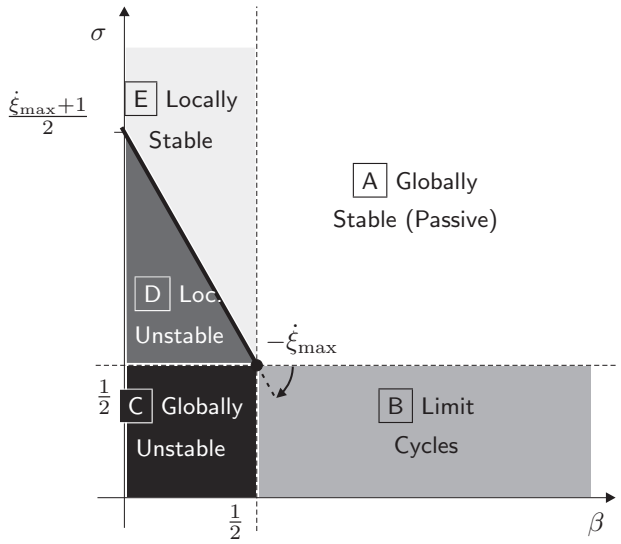

Figure 8.8: Dimensionless stability plane with characteristic regions for zero delay where $\beta := \frac{b}{KT}$ and $\sigma := \frac{c}{K\Delta}$ and $\dot{\xi}(\tau) = \frac{\dot{x}T}{\Delta}$ [Diolaiti et al. 06]. (© 2006 IEEE)

If at sample times t_{k-2} and t_{k-1} the position information remains constant, $\hat{v}_{k-1} = 0$. However, if at sample time t_k the position increases by one quanta, δ, then the resulting velocity suddenly jumps to a very large value, $\hat{v}_k = \frac{\delta}{T}$. This rapidly varying velocity estimate can lead to instability. One common method to reduce this effect is to low-pass filter the resulting velocity signal, thereby smoothing out the jumps. With increasing sample rate, filtering becomes more imperative to obtain velocity signals. This presents a trade-off, however, as increased filtering leads to increased time delay and phase distortion, which can cause instability. The precision of the velocity estimate improves with decreased sample rate, as illustrated in Figure 8.9. However the reliability of the signal decreases due to the longer time delay. This has the effect of averaging the velocity over a longer period of time, or over a number of samples, as shown in Figure 8.9 and Equation 8.23.

$$\hat{v}_k = \frac{1}{n}\sum_{j=0}^{n-1} \hat{v}_{k-j} = \frac{y_k - y_{k-n}}{nT} \tag{8.23}$$

Fixed filters, such as a Butterworth filter, compute velocity from a weighted sum of the raw velocity signal, $\hat{v}_j^{'}$, and past filtered velocity estimates, $\hat{v}_j$.

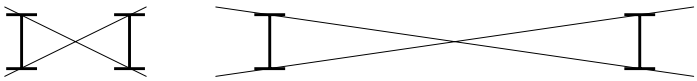

Figure 8.9: Effect of window length on the variance of velocity [Janabi-Sharifi et al. 00]. ()

$$\hat{v}_k = \sum_{j=0}^{n} b_j \hat{v}'_{k-j} + \sum_{j=1}^{n} a_j \hat{v}_{k-j} \tag{8.24}$$

where a_j and b_j are the filter coefficients, and n is the order of the filter. As n increases, the filter becomes more like an ideal low-pass filter; however the delay and phase distortion are also increased. An additional subtlety is that the signal is filtered along with the noise, so that heavy filtering leads to poor transient response. To address this, [Janabi-Sharifi et al. 00] introduce a velocity filtering technique that relies on a first-order adaptive window length. The basic concept is that, when position signals are changing slowly, the window should be long to provide a precise estimate of the velocity. However, when the position is rapidly changing, the window length should be short to improve velocity reliability and prevent introduction of excessive delay. The window criterion exists to determine whether the slope of a straight line reliably approximates the derivative of the signal between two samples, x_k and x_{k-n}. If the noise, d, in the position signal can be assumed to be uniformly distributed, such that $d = \|e_k\|_\infty \; \forall k$, then mathematically, the adaptive window problem becomes finding a solution for the largest possible window length n that satisfies the following:

$$|y_{k-i} - L_{y_{k-i}}| \leq d, \qquad \forall i \in \{1, 2, \ldots, n\} \tag{8.25}$$

$$\text{where} \quad L_{y_{k-i}} = a_n + b_n(k-i)T, \qquad \text{given that} \tag{8.26}$$

$$a_n = \frac{k y_{k-n} + (n-k) y_k}{n} \qquad \text{and} \tag{8.27}$$

$$\hat{v}_k = b_n = \frac{n \sum_{i=0}^{n} y_{k-i} - 2 \sum_{i=0}^{n} i y_{k-i}}{T n(n+1)(n+2)/6} \tag{8.28}$$

The solution for the window length, n, is found iteratively where the window grows from $n = 1$ until the window no longer fits the enclosed data; then the previous n is used to compute the velocity estimate. b_n is the slope of a line that is a least-square approximation that minimizes the error in the velocity signal [Janabi-Sharifi et al. 00].

8.4.2 Nonlinearities

Nonlinearities are an important consideration for haptic displays in virtual environments. Essentially, almost all useful virtual environments are nonlinear in that impedances change dramatically upon contact with objects in the virtual environment. [Miller et al. 00] analyze the passivity of nonlinear delayed and non-delayed virtual environments. The authors establish a passivity criterion relating the haptic display and human operator, the virtual coupling, and the virtual environment for both delayed and non-delayed environments. Virtual couplings will be introduced in more detail in Part II of this chapter.

Again, the physical dissipation in the mechanism is a critical parameter. In addition to the passivity criterion, a key result is a limit to an environment parameter, α, measuring the lack of passivity exhibited by the virtual environment. It can be expressed as a function of inertia, damping and stiffness parameters. α is related to the physical dissipation in the system, δ, and is modulated by the impedance of the virtual coupling γ, if present [Miller et al. 00]:

$$\alpha < \delta \tag{8.29}$$

$$\alpha < \frac{\delta\gamma}{\delta+\gamma} \tag{8.30}$$

Many common haptic devices also have nonlinear kinematics. Through an analysis of system dynamics, [Miller et al. 04] shows how the nonlinear transformation from joint space to task space for a haptic display also affects passivity. This result can be summarized by the following inequality:

$$\delta_m \geq J^T \delta J \tag{8.31}$$

where δ_m represents the joint space dissipation, J is the haptic interface Jacobian, and δ is the task space dissipation required for passive rendering of the desired virtual environment.

8.5 Control Methods

8.5.1 Virtual Coupling

Virtual coupling is one of the basic techniques for rendering virtual environments in haptics, introduced by [Colgate et al. 95] and amplified by [Miller et al. 00, Adams and Hannaford 98] and others. The virtual coupling connects the haptic display and the virtual environment, and consists

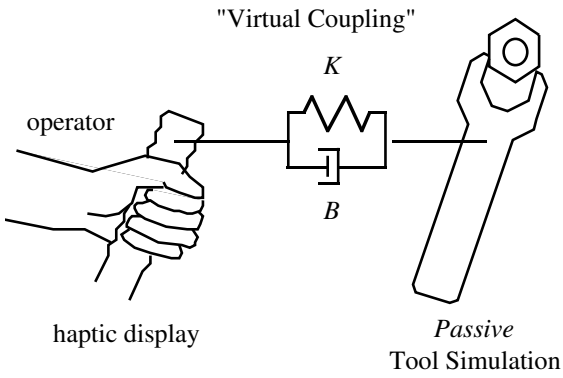

Figure 8.10: The virtual coupling [Colgate et al. 95]. (© 1995 IEEE)

of a virtual spring in virtual damper in mechanical parallel, as shown in Figure 8.10.

The virtual coupling is advantageous because it simplifies the problem of ensuring stability. Using a virtual coupling to establish stability of the haptic display, which is a sampled-data system, it is only necessary to satisfy the following two conditions:

1. Select the virtual coupling parameters, such that a virtual wall with these parameters would be passive.

2. Make the virtual environment discrete-time passive.

Condition 2 is simpler to achieve than analyzing the complete sampled-data system to ensure passivity. Separating the discrete-time passivity of the virtual environment from the rest of the system frees the designer from concerns regarding the interaction between the virtual environment and the haptic display and human operator. The virtual coupling, however, has the effect of reducing the maximum environment impedance to match the passivity limits of the haptic display, which are generally lower than the impedances of the virtual environment.

Virtual environments rendering mass require the use of discrete time integrators which typically are not passive, making condition 2 difficult to meet. [Brown and Colgate 98] analyzed various discrete time integration techniques in the context of establishing the lower bound of virtual mass that can be rendered while maintaining passivity. The value of minimum mass required for passive rendering depends on the form of integrator used.

The work of [Miller et al. 00] generalized these results by explicitly modeling the non-passivity of the human and haptic interface as well as the

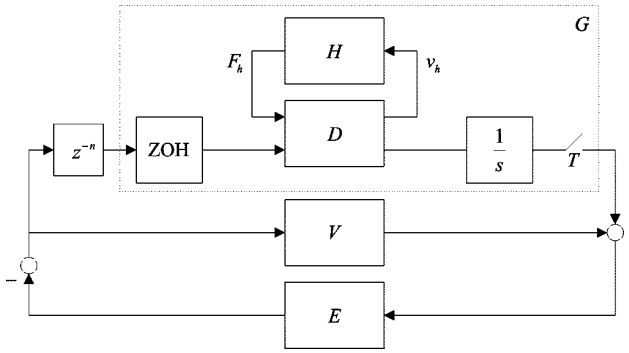

Figure 8.11: The haptic display system with a virtual coupling [Miller et al. 00]. (© 2000 IEEE)

virtual environment (Figure 8.11). As shown in Equation 8.30, the virtual coupling increases the allowed lack of passivity in the virtual environment while still maintaining overall system passivity.

[Adams and Hannaford 98] introduced the use of a virtual coupling network to analyze and guarantee system stability. Using this technique, elements of the haptic display are typically modeled as a series of interconnected, two-port elements in a network, shown in Figure 8.12. The virtual coupling introduced by [Colgate et al. 95] and the coupling behavior of the god-object introduced by [Zilles and Salisbury 95] are subsets of this more general two-port coupling network approach. Coupling network results are shown for both admittance and impedance architectures. This technique was then applied to a 2 degree of freedom haptic display in both impedance and admittance configurations, showing passivity results derived experimentally and theoretically for both conditions [Adams et al. 98].

8.5.2 Passivity Observers and Controllers

[Gillespie and Cutkosky 96] introduced a technique for stabilizing virtual walls by compensating for the energy leaks due to the zero order hold as well as the asynchronous switching times associated with sampling. Asynchronous switching times arise because the haptic display generally does not enter or exit the virtual wall exactly at a sampling time; typically the transition from "outside" to "inside" the virtual wall occurs in between sampling intervals (Figure 8.3). These two sources of error are treated separately. The goal is to design a digital controller to cancel the effects of these induced energy leaks, stabilizing the system. Figure 8.13-A shows a

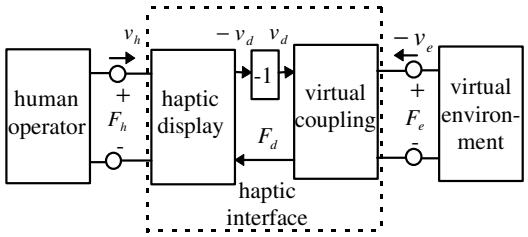

Figure 8.12: The virtual coupling as a two-port element in a network [Adams and Hannaford 98]. (© 1998 IEEE)

sampled-data system simulation of a ball bouncing on a surface, without sampling correction.

The dominant behavior of the zero order hold can be approximated as a half sample delay. By designing a controller that predicts the state of the system one half sample forward in time, the majority of the error introduced by the zero order hold can be canceled. At sample time $t = kT$, the controller predicts the state at $t = KT + T/2$ and then renders the virtual environment using the predicted system state. Figure 8.13-B shows simulation results using a half sample prediction algorithm of a sampled-data system rendering a bouncing ball. It can be seen that modeling the zero order hold as a half sample delay improves the rendering during the majority of the time the ball is in contact with the virtual wall. However, during the last sample and while in contact with the wall, the algorithm introduces an error, computing a force pulling back toward the wall. This error occurs because the ball exits the virtual wall between sampling intervals due to the secondary effect of sampling, asynchronous switching times.

To address this second concern, a model of the system to predict threshold crossing times using state information is also incorporated. Conceptually, this is estimating t_a and t_b in Figure 8.3, given a model of the known properties of the system and virtual environment being rendered. Deadbeat control is then used to compensate for the energy leaks caused by these asynchronous switching times. Figure 8.13-C shows the final improvement after correcting the half sample delay and using deadbeat control to correct for asynchronous switching times. Note that correcting for the effects of sampling is independent of the added problem of sensor quantization.

Expanding on this work and the work on virtual coupling networks, [Hannaford et al. 01] introduced passivity observers (POs) and passivity controllers (PCs) for stabilizing haptic interaction with virtual environments. Passivity observers analyze system behavior and track the energy

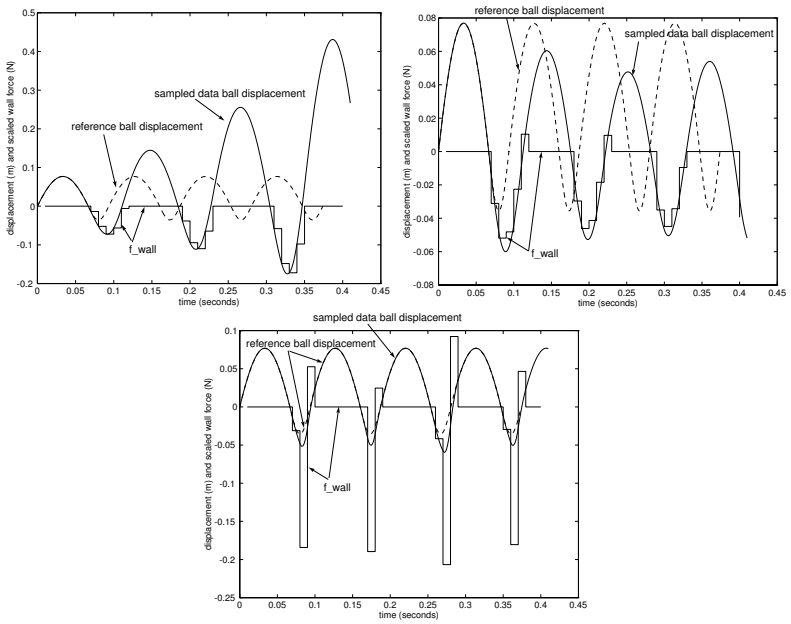

Figure 8.13: (a) Sampled-data system simulation of a bouncing ball. (b) Half sample prediction simulation results of a bouncing ball. (c) Bouncing ball simulation with sampling and zero order hold correction algorithm active. [Gillespie and Cutkosky 96]

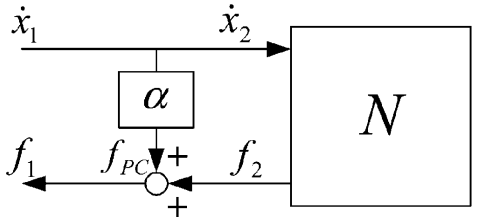

Figure 8.14: One-port network with passivity controller [Ryu et al. 04]. (© 2004 IEEE)

flow between elements to estimate errors introduced into the sampled-data system. Passivity controllers act to dissipate this excess energy by adjusting the impedance between elements in the system (Figure 8.14). They effectively inject additional damping to dissipate energy.

One of the main advantages of POs is that the PC does not modify the

desired system impedance unless an energy correction is necessary. Unlike the virtual coupling, which constantly moderates the feel of the virtual environment, the passivity controller adds damping only when necessary to counteract energy leaks. This can potentially lead to better feeling virtual environments.

The earliest POs assumed that velocity and force was constant between samples, but more recent passivity observers presented in [Ryu et al. 05], based on [Ryu et al. 04] and [Stramigioli et al. 02], show that this assumption can be relaxed. The resulting passivity observer for an impedance causality device takes the following form:

$$E_{obsv}(k) = \left[\sum_{j=0}^{k} f(t_{j-1})(x(t_j) - x(t_{j-1}))\right] + f(t_j)(x(t_j) - x(t_{j-1})) \quad (8.32)$$

The bracketed term of Equation 8.32 represents the exact energy input to the discrete-time virtual environment from time 0 to time t_k, and the second term is an estimate of the energy input one time step ahead, and based on the assumption that the velocity does not change during that time step. If the dynamics of the controller are much faster than the dynamics of the mechanical system, then the predictive second term in Equation 8.32 is typically not necessary. If at any time the observed energy, E_{obsv}, is negative, then the sampled-data system may be contributing to instability. It is then the job of the PC to modify the impedance of the network to dissipate the excess energy.

To further improve the performance of PO/PC systems and maintain the perception of a good feeling virtual environment, the excess energy should be dissipated smoothly. [Ryu et al. 05] introduced a PO that smoothly corrects for energy leaks by modeling the behavior of a reference system and comparing that to the observed behavior, shown in Figure 8.15. For simple virtual environments, a model of the energy flow into the virtual environment can be explicitly calculated to act as the reference energy. However, most interesting virtual environments are nonlinear, making an exact calculation of the energy flow into the virtual environment very difficult. In this case and in the case of designing a general passivity observer, a simple energy model can be used to reference the behavior. One implementation of such an energy tracking reference is the numerical integration of the power flow into the virtual environment, where the force is computed given the observed position information.

In the case of a continuous and lossless one-port network system, the energy input to the system should be equal to the energy stored, S, plus the energy dissipated, D:

$$\int_0^t f(\tau)\dot{x}(\tau)d\tau = S(t) + D(t), \quad \forall t \geq 0 \tag{8.33}$$

This leads to the following PC algorithm for the one-port network with impedance causality shown in Figure 8.14 [Ryu et al. 05]. In this case, the PO (E_{obsv} in step 4, Equation 8.34) uses the modeled energy, instead of the one step ahead predicted energy in Equation 8.32.

1. $x_1(k) = x_2(k)$ is the input.
2. $\Delta x(k) = x_1(k) - x_1(k-1)$
3. $f_2(k)$ is the output of the one-port network.
4. The actual energy input at step k is:

$$E_{obsv}(k) = \sum_{j=0}^{k} f_1(j-1)\Delta x(j) \tag{8.34}$$

5. $S(k)$ and $D(k)$ are the amount of stored energy and dissipated energy of the virtual environment at step k, respectively.
6. The PC control force to make the actual input energy follow the reference energy is calculated:

$$f_{PC}(k) = \begin{cases} \frac{-(E_{obsv}(k)-S(k)-D(k))}{\Delta x(k)} & \text{if} \quad W(k) < 0 \\ 0 & \text{if} \quad W(k) \geq 0 \end{cases} \tag{8.35}$$

   where $W(k) = E_{obsv}(k) - S(k) - D(k)$.
7. $f_1(k) = f_2(k) + f_{PC}(k)$ is the output.

Another improvement to the passivity observer gained by following the energy of a reference system is the problem of resetting. Consider the case of a virtual environment that is both highly dissipative in certain regions and active in other regions. The active region requires the passivity controller to add damping to maintain stability. If the user spends a long time in the dissipative region before contacting the active region, a large accumulation of positive energy in the passivity observer can be built up during interaction with the dissipative region. This is very similar to the problem of integrator wind-up. Upon switching to the active region, the passivity observer may not act until the net energy becomes negative, causing a delay while the accumulated excess of passivity is reduced. During that delay, the system can exhibit unstable behavior. If the passivity observer tracks a reference energy system, this problem of resetting can be avoided.

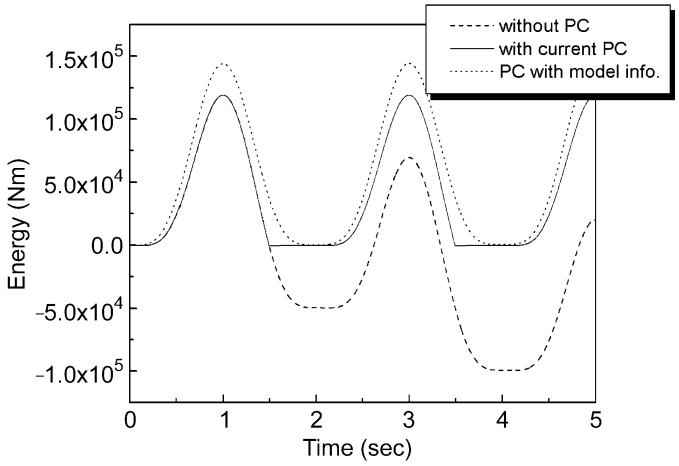

Figure 8.15: Effect of passivity controller and modeled reference energy [Ryu et al. 05]. (© 2005 IEEE)

Another method of tracking and dissipating energy leaks is presented by [Stramigioli et al. 02]. This work uses a port-Hamiltonian method for estimating these sampled-data system errors. The key aspect of all of these energy leak and passivity controllers is determining the inaccuracy introduced by the discrete-time approximation of the continuous system, so that the controller can dissipate this excess energy.

8.6 Extending Z-Width

This section first extends the passivity criterion in Equation 8.2, and gives insight into passivity design with frequency-dependent damping. Then, mechanical and electrical methods of implementing high frequency damping are reviewed.

8.6.1 Frequency-Dependent Passivity Criterion

A system in feedback with an uncertainty set consisting of all possible passive behaviors must itself be strictly passive to guarantee closed loop stability [Colgate and Hogan 88]. We use this fact to establish the strict passivity of the haptic display model in Figure 8.16. Specifically, we replace the block representing the human operator with a block containing the uncertainty set Σ. Σ is the set of all linear, time-invariant (LTI), passive

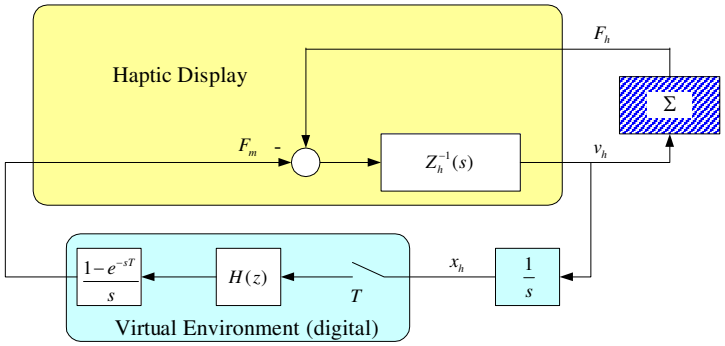

Figure 8.16: Model of a haptic system. Z_h is the impedance of the haptic display hardware; $H(z)$ is the (linear) virtual environment; Σ is the uncertainty set that we use to replace the human operator. Note that we assume the actuator force F_m and human force F_h are collocated.

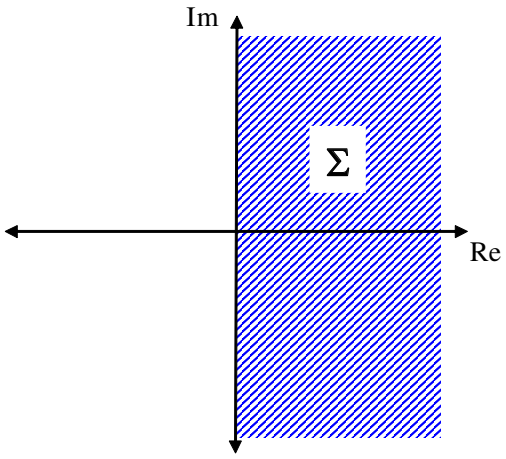

Figure 8.17: The set of all possible LTI passive impedances occupies the right half Nyquist plane.

operators that map v_h to F_h. It is well-known that such an operator must be positive real; i.e., in the Nyquist plane, the real part (representing energy dissipation) must be non-negative. Thus, Σ can be represented by the half-plane shown in Figure 8.17.

The task, therefore, is to prove the stability of the system illustrated in

Figure 8.16. Doing so establishes the strict passivity of the haptic display. In this section, we only outline the proof, which uses Nyquist theory. The basic strategy is to write the closed loop characteristic equation as $1 + A(s)\Delta(s) = 0$, where $\Delta(s)$ is the uncertainty set consisting of the unit disk. If the open loop (uncoupled) system is stable, then a sufficient condition for closed loop (coupled) stability is:

$$1 + A(j\omega)\Delta(j\omega) \neq 0 \qquad \forall\omega, \forall\Delta \tag{8.36}$$

or, equivalently,

$$|A(j\omega)| < 1 \qquad \forall\omega \tag{8.37}$$

This is a version of the Small Gain Theorem [Desoer and Vidyasagar 75].

Straightforward manipulation shows that the sufficient condition for the closed loop stability of Figure 8.16 is:

$$1 - H(e^{j\omega T})\frac{1 - e^{-j\omega T}}{T}\sum_{n=-\infty}^{n=\infty}\frac{1}{[Z(j\omega + jn\omega_s) + \Sigma(j\omega + jn\omega_s)](\omega + n\omega_s)^2} \neq 0 \tag{8.38}$$

where $\omega_s = 2\pi/T$ is the sample rate. Consider the sum $Z + \Sigma$. Because Σ has an arbitrary imaginary part, the imaginary part of Z contributes nothing further. The real part of Z, however, shifts Σ to either the right or left, depending on sign. In the cases of interest, $\Re\{Z(j\omega)\} > 0$, which shifts Σ to the right. Moreover, $1/(Z + \Sigma)$ is easily found to be a circular disk centered on the real axis and tangent to the origin as well as the point $(1/\Re\{Z(j\omega)\}, 0)$. If this disk were frequency independent, we could factor it out of the infinite sum, but in general this is not the case. Here, we will make the assumption that $\Re\{Z(j\omega)\}$ is non-decreasing with frequency, meaning that the amount of damping in the haptic display remains fixed or grows with increasing frequency. With this assumption, it is apparent that:

$$\frac{1}{Z(j\omega + jn\omega_s) + \Sigma(j\omega + jn\omega_s)} \subset \frac{1}{\Re\{Z(j\omega)\} + \Sigma(j\omega)} \qquad \forall n \neq 0 \tag{8.39}$$

And Equation 8.38 is satisfied whenever Equation 8.40 holds true:

$$1 + H(e^{j\omega T})\frac{1 - e^{-j\omega T}}{T[\Re\{Z(j\omega)\} + \Sigma(j\omega)]}\sum_{n=-\infty}^{n=\infty}\frac{1}{(\omega + n\omega_s)^2} \quad \neq \quad 0 \tag{8.40}$$

The infinite sum can be solved analytically, yielding:

$$1 + H(e^{j\omega T})\frac{T(1 - e^{-j\omega T})}{2(1 - \cos(\omega T))[\Re\{Z(j\omega)\} + \Sigma(j\omega)]} \quad \neq \quad 0 \tag{8.41}$$

Or, in terms of the unit disk, Δ:

$$1 + H(e^{j\omega T})\frac{T(e^{-j\omega T} - 1)}{4(1 - \cos(\omega T))}\frac{1 + \Delta}{\Re\{Z(j\omega)\}} \quad \neq \quad 0 \tag{8.42}$$

For compactness, we define:

$$r(j\omega) = \frac{T(e^{-j\omega T} - 1)}{4(1 - \cos(\omega T))} \tag{8.43}$$

The assumption of uncoupled stability enables us to rewrite Equation 8.42 as:

$$1 + \frac{r(j\omega)H(e^{j\omega T})}{\Re\{Z(j\omega)\} + r(j\omega)H(e^{j\omega T})}\Delta \quad \neq \quad 0 \tag{8.44}$$

which is the form of Equation 8.36. Thus, stability requires:

$$\left|\frac{r(j\omega)H(e^{j\omega T})}{\Re\{Z(j\omega)\} + r(j\omega)H(e^{j\omega T})}\right| \quad < \quad 1 \tag{8.45}$$

This can be manipulated into the following form:

$$\Re\{Z(j\omega)\} \quad + \quad \frac{T}{2(1 - \cos(\omega T))}\Re\{(e^{-j\omega T} - 1)H(e^{j\omega T})\} > 0 \tag{8.46}$$

$$\text{for} \quad 0 \leq \omega \leq \omega_N = \frac{\omega_s}{2} \tag{8.47}$$

Equation 8.46 may be compared to the result of [Colgate and Schenkel 97], also presented here as Equation 8.2. In the event that $\Re\{Z(j\omega)\}$ has a fixed value of b, the results are the same. Equation 8.46 is therefore a more general result than previously reported, but subject to the non-decreasing assumption.

8.6.2 Insights into Passivity and Damping

The passivity criterion in Equation 8.46 is slightly more general than Equation 8.2 in that it allows for frequency-dependent physical damping, but only under the assumption that the physical damping is a non-decreasing function of frequency.

The criterion in Equation 8.46 lets us, in effect, sum together the physical damping (first term) and virtual damping (second term). At each

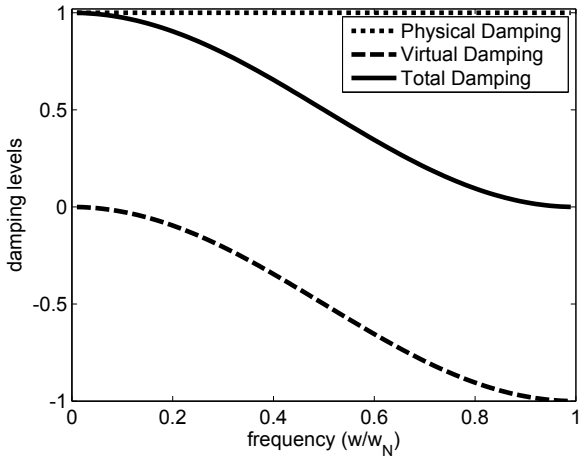

Figure 8.18: Physical, virtual, and total damping levels for the system of Figure 8.19a and the virtual wall of Equation 8.3 with $m/b = 0.1$, $KT/b = 1$, $B/b = 0.5$. Note the excess of total damping at low frequency required to achieve positive damping at the Nyquist frequency.

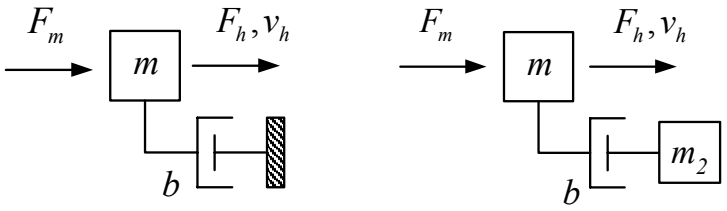

Figure 8.19: (a) Model of a haptic display having inertia m and viscous damping b. (b) Addition of the mass m_2 gives rise to "high pass" damping.

frequency from zero to the Nyquist frequency, the sum (total damping) must be positive to ensure passivity.

Figure 8.18 shows, as an example, the physical, virtual, and total damping for the haptic display pictured in Figure 8.19a, and implements the virtual wall of Equation 8.3. It is evident that, in order to ensure passivity at the Nyquist frequency, a considerable excess of damping is required at low frequencies.

The negative virtual damping at high frequency is caused principally by the phase delay of the backwards difference differentiator used to compute

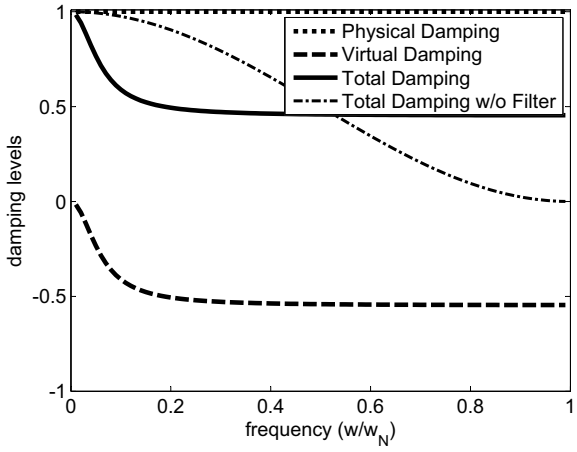

Figure 8.20: Physical, virtual, and total damping for the system of Figure 8.19a, with the same parameters as Figure 8.18 and the addition of a first order low pass velocity filter having a cutoff frequency one-fifth of the Nyquist frequency. Note that the improved total damping at high frequencies is offset by reduced total damping at low frequencies. Nonetheless, it is evident that the physical damping could be reduced or the virtual wall impedance increased without loss of passivity.

velocity. This effect can be minimized by filtering. For instance, if we combine a first order low-pass digital filter with the differentiator, and set the cutoff frequency at one fifth the Nyquist frequency, we obtain Figure 8.20. The high frequency negative damping has been reduced but at a cost. The extra phase lag introduced by the filter causes negative virtual damping to occur at lower frequencies. This is a good illustration of why high order velocity filters are rarely used in haptics: the cost of added phase delay often out-weighs the benefits of magnitude roll-off. To the best of the author's knowledge, no theory of optimal filter design for haptics (other than the work of [Janabi-Sharifi et al. 00] reviewed previously, which is aimed at handling quantization), has been developed.

A second approach to improving Z-width is to replace the simple, fixed damper of Figure 8.19a with a high frequency damper, such as the one in Figure 8.19b. By connecting the distal end of the damper to a floating inertia rather than to ground, the effective physical damping, $(\Re\{Z(j\omega)\})$ approaches zero at low frequency. Figure 8.21 shows that the combination of "high pass" damping and velocity filtering enables a significantly higher impedance virtual wall to be implemented passively than for the naïve

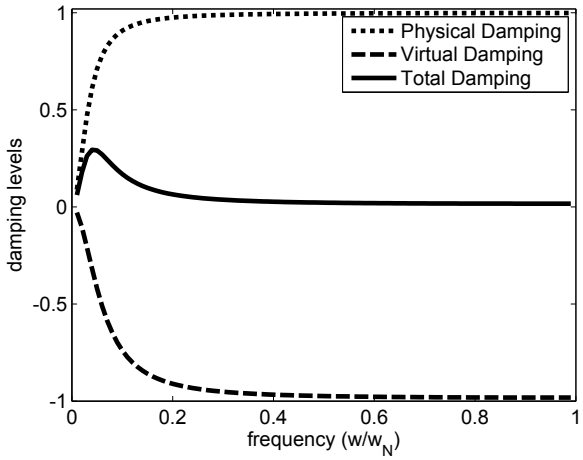

Figure 8.21: Physical, virtual, and total damping for the system of Figure 8.19b, with the same low pass velocity filter as Figure 8.20, and a higher impedance virtual wall. Parameters are $m/b = 0.1$, $m_2/b = 0.01$, $KT/b = 1.8$, $B/b = 0.9$. Positive total damping is maintained at all frequencies without significant excess at any frequency.

design of Figures 8.18 and 8.19a.

8.6.3 Mechanical Methods

The direct approach of adding a mechanical viscous damper to the haptic interface to increase the maximum passive impedance of the system works well, as demonstrated by [Colgate and Brown 94]. The maximum passive virtual stiffness and damping are limited by the physical dissipation in the mechanism by Equation 8.4. The additional physical damping is counteracted using digital control; the damper torque is measured and a low-passed version of this torque is added to the motor command. This masks the user's perception of damping at the low frequencies of human voluntary motion, but improves system stability and passivity at high frequencies where discrete-time control is ineffectual and energy leaks are most problematic.

There are some practical problems with typical physical dampers, such as temperature dependence, fluid leakage, and Coulomb friction generated in fluid seals. Figure 8.4 shows the increased impedance range when physical damping is added to the haptic display and when the sampling rate is increased. Magnetic dampers using eddy currents also work with the

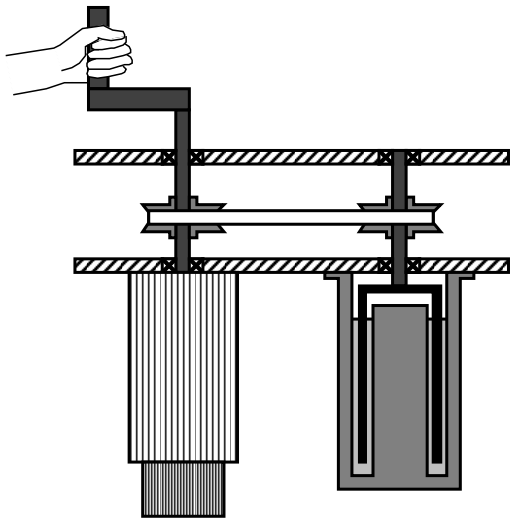

Figure 8.22: Design of a 1 DOF Haptic Display with motor (on the left) and fluid filled viscous damper (on the right) connected via a removable steel tape [Brown 95].

added benefit of being able to turn off the damping, when rendering low impedances [Gosline et al. 06]. It is also possible to use mechanical brakes to dissipate energy and mimic the behavior of a damper in order to provide the necessary dissipation in the mechanism [An and Kwon 06], although the slow dynamic response of magnetic brakes may limit their performance.

8.6.4 Electrical Methods

More recently, a variety of techniques emerged that take advantage of analog components for rendering continuous time behavior. This method strives to avoid the difficulties presented by mechanical dampers, but still incorporates the dramatic performance improvements afforded.

One such method of electrically increasing the Z-width of a haptic display is to design an analog motor controller that locally monitors each joint and controls the coupling stiffness and damping [Kawai and Yoshikawa 02] in order to maintain passivity. A schematic of this is shown in Figure 8.23. In this way, the joint stiffness and damping are continuously controlled, while the virtual environment is updated and commands the joint coupling parameters at the sampling intervals, as shown in Figure 8.24. The increase in passivity and system Z-width using these analog impedance controllers is shown in [Kawai and Yoshikawa 04].

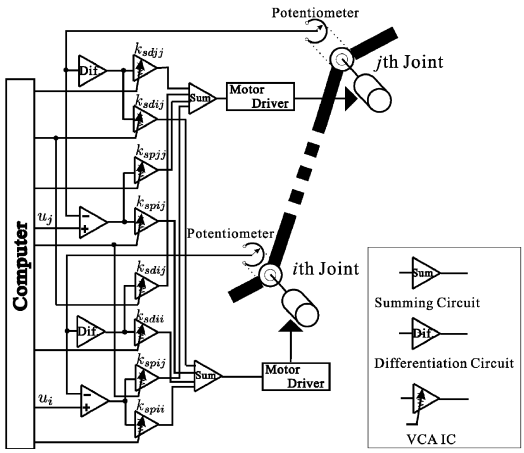

Figure 8.23: Outline of analog feedback control corresponding to two joints [Kawai and Yoshikawa 04]. (© 2004 IEEE)

Another class of controllers takes advantage of the motor's natural dynamics. Since electric motors are gyrators, a damper on the mechanical side of the motor acts as a resistor on the electrical side of the motor [Karnopp et al. 00]. [Mehling et al. 05] used a resistor and capacitor in parallel with the motor to add frequency dependent electrical damping to a haptic display, as illustrated in Figure 8.25.

The amount of electrical damping added is a function of the motor torque constant K_t, the motor winding resistance R_m, and the external resistor R_1:

$$b_{eq} = \frac{K_t^2}{R_1 + R_m} \tag{8.48}$$

This technique can be quite effective as illustrated in Figure 8.26. [Mehling et al. 05] used an R-C cutoff frequency of 2.6 Hz, providing significant damping at higher frequencies where the haptic display is likely to be unstable or exhibit limit cycle oscillations and above the frequencies of human voluntary motion. It is important to note that the capacitor acts as apparent inertia on the mechanical side of the motor. For this reason, the R-C time constant of the electrical damper must be selected carefully. The resistance must be small enough to provide useful damping at the frequencies of interest, while keeping the capacitance small enough to cause only a modest impact on apparent inertia at low frequency.

Clearly, maximum physical damping, b, is provided when R_1 goes to

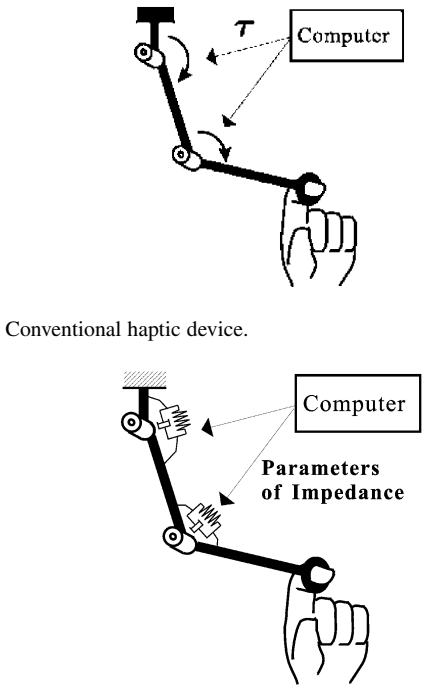

Figure 8.24: Conventional and electrically coupled hybrid haptic device [Kawai and Yoshikawa 04]. (© 2004 IEEE)

zero, i.e. the motor is "crowbarred." However, this creates problems with driving the motor; any voltage applied bypasses the motor. The winding resistance, R_m, also sets an upper bound on the electrical damping that can be achieved in this configuration. There is also a practical limit to how large the capacitance can be in addition to the added apparent inertia at low impedance.

To increase electrical damping beyond the limit of Equation 8.48, it is possible to design a circuit to cancel the effect of the motor winding resistance, R_m [Diolaiti and Niemeyer 06]. Such a circuit in the motor amplifier allows the motor winding resistance to be reduced dramatically; however, due to noise and thermal effects, R_m cannot be canceled completely. Due to gyration, the motor winding inductance acts like a spring on the mechanical side. [Diolaiti and Niemeyer 06] take advantage of this by combining wave variable control with a circuit to cancel R_m, leaving

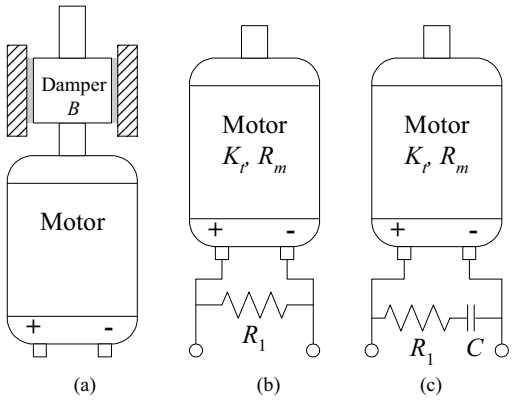

Figure 8.25: A mechanically damped system (a) and two electrically damped systems; one without (b) and one with frequency dependence (c) [Mehling et al. 05]. (© 2005 IEEE)

the springlike inductance to couple the physical world with the virtual environment. The benefit is that for common DC motors, such as those in the Phantom haptic display, the resulting effective spring constant of the inductance is much higher than the maximum passive stiffness that can be attained using feedback and digital control. This technique also requires recasting the digital controller in the form of wave variables, as shown in Figure 8.27.

Extending Diolaiti and Niemeyer's work, it is possible to use analog circuitry to estimate the back EMF (electromotive force or voltage) of the winding, by canceling both the resistance and the inductance of the motor windings. The back EMF of the motor is proportional to velocity, so feeding this signal back to the motor inside the current control amplifier provides electrical damping. One caveat is that prior knowledge of the parameters and dynamics of the motor is required in order to design such circuitry, and dynamic tuning of the parameters is necessary to compensate for heating in the windings.

8.6.5 Psychophysical Methods

In addition to analytical and quantitative methods for increasing the maximum passive stiffness that can be rendered by a haptic display, there are a variety of psychophysical techniques available to improve human perception of stiff virtual surfaces.

[Salcudean and Vlaar 97] developed a rendering method for virtual

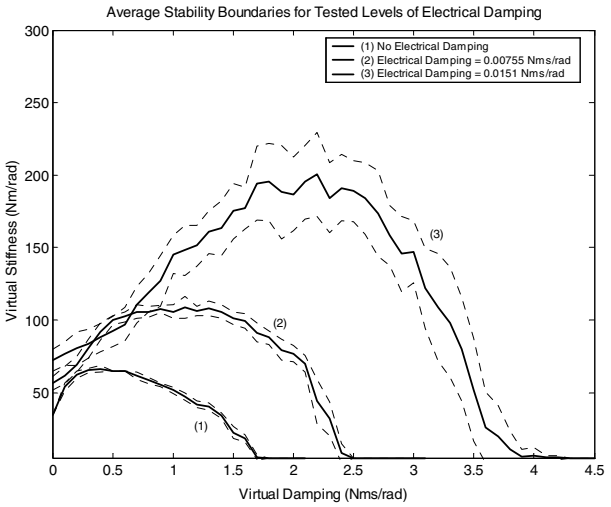

Figure 8.26: Z-width plot of the average stability boundary for each level of electrical damping. Dashed lines indicate plus or minus one standard deviation [Mehling et al. 05]. (© 2005 IEEE)

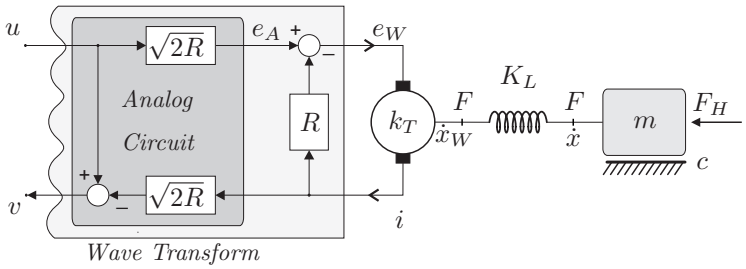

Figure 8.27: The wave transform connecting the virtual environment to the electrical domain is implemented with an analog circuit [Diolaiti and Niemeyer 06]. (© 2006 IEEE)

walls using a "braking pulse" that occurs upon contact with the wall boundary. The force of the pulse is designed to bring the haptic display to rest as quickly as possible, ideally in one sampling period. This corresponds to a very high level of damping when crossing the wall boundary, but since the high level of damping is not sustained, it does not lead to instability that would occur with a similar level of virtual damping in a constant

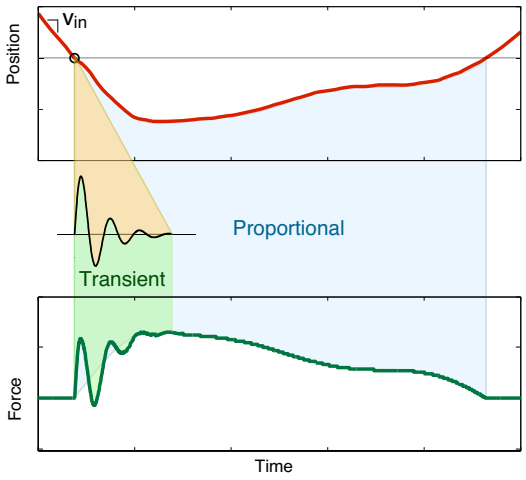

Figure 8.28: Schematic of position and force in event-based haptic display [Kuchenbecker et al. 06]. (© 2006 IEEE)

parameter virtual wall. After the braking pulse, as the user remains in contact with the virtual wall, the rendering method consists of the standard spring-damper virtual wall with virtual stiffness and damping gains set, such that they are stable. This results in behavior that is similar to an object colliding with a real wall and increases the perceived wall stiffness.

[Lawrence et al. 00] introduced the concept of "rate-hardness" as a way of quantifying human perception of our virtual surfaces. Rate-hardness is the ratio of initial rate of change of force versus initial velocity upon penetrating the surface. Human perception studies indicate that rate-hardness is a more relevant perceptual hardness metric then absolute mechanical stiffness when rendering virtual surfaces. This is likely due to the relatively poor performance of the human kinesthetic sense when in contact with stiff walls. When a human is already in contact with a stiff virtual wall, the change in position relative to the change in force when haptically querying the wall is very small.

If the user is allowed to dynamically test the wall through tapping, for example, human perception is much better at distinguishing varying surface hardness. It seems that tapping elicits high frequency force differences which can be perceived by the pressure and vibration sensory receptors in the fingers. Artificially increasing the rate hardness can act as a haptic illusion, making the surface seem harder than the stiffness alone would predict [Lawrence et al. 00].

[Okamura et al. 98] introduced a technique to improve the perception of contact with virtual objects. High frequency open-loop force transients corresponding to interaction events in the virtual environment are superimposed on a standard virtual wall controller, as indicated in Figure 8.28. To determine the open loop vibrations to display, high resolution vibration and position information was gathered while tapping on a variety of materials. The data was fit to the amplitude $A(v)$, decay constant B, and frequency ω of a decaying sinusoidal signal $Q(t)$, resulting in each material having a different vibration signature.

$$Q(t) = A(v)e^{-Bt}\sin(\omega t) \tag{8.49}$$

Typical haptic displays generally do not accurately reproduce high frequency vibration signals. To compensate for these device dynamics, [Okamura et al. 01] improved the vibration models by performing a set of human perceptual experiments to tune the parameters of the vibration signatures. Based on the results of the experiments, the adjusted parameters result in more realistic perception of tapping on the three test materials: rubber, wood, and aluminum. One drawback to these techniques is that each material type, geometry, and haptic display needs to be individually characterized prior to use to determine appropriate vibration signatures.

Extending the work on reality-based vibration feedback, [Kuchenbecker et al. 06] utilized an acceleration matching technique based on the experience of contacting the real object being rendered in the virtual environment. To improve the accuracy of the force transients displayed upon contact with a virtual object, the open-loop acceleration signal is pre-warped by an inverted system model to correct for the distortion and dynamics induced by the haptic display. Chapter 22 treats in more detail measurement-based haptic rendering.

8.7 Summary

In summary, haptic instability frequently arises from a lack of passivity when rendering virtual environments. In order to maintain passivity, virtual environment impedance can be reduced to acceptable levels for passivity, but this depends upon the specific hardware used, and highly complex virtual environments make this undesirable. To preserve the universality and accuracy of virtual environments, virtual couplings can be used to modulate the impedance transmitted between the haptic display and the virtual environment to ensure passivity. Passivity controllers can increase the nominal impedance of haptic display by counteracting energy leaks introduced by the sampled-data system. Direct methods of design-

ing for passivity work to increase the maximum passive impedance of the haptic interface, improving performance. Lastly, perceptual methods of improving performance take advantage of the limits of human perception to create the illusion of higher performance rendering on existing haptic display hardware.

Acknowledgements This work was supported in part by Northwestern University, National Science Foundation IGERT Fellowships through grant DGE-9987577, and National Science Foundation Grant No. 0413204.

Bibliography

[Abbott and Okamura 05] Jake J. Abbott and Allison M. Okamura. "Effects of Position Quantization and Sampling Rate on Virtual-Wall Passivity." *IEEE Transactions on Robotics* 21 (2005), 952–964.

[Adams and Hannaford 98] Richard J. Adams and Blake Hannaford. "A Two-Port Framework for the Design of Unconditionally Stable Haptic Interfaces." In *IEEE/RSJ International Conference on Intelligent Robots and Systems*, 2, 2, pp. 1254–1259. Victoria, BC, Canada: IEEE, 1998.

[Adams and Hannaford 99] Richard J. Adams and Blake Hannaford. "Stable Haptic Interaction with Virtual Environments." *IEEE Transactions on Robotics and Automation* 15 (1999), 465–474.

[Adams et al. 98] Richard J. Adams, Manuel R. Moreyra, and Blake Hannaford. "Stability and Performance of Haptic Displays: Theory and Experiments." In *Proceedings ASME International Mechanical Engineering Congress and Exhibition*, pp. 227–234. Anaheim, CA: ASME, 1998.

[An and Kwon 06] Jinung An and Dong-Soo Kwon. "Stability and Performance of Haptic Interfaces with Active/Passive Actuators-Theory and Experiments." *International Journal of Robotics Research* 25:11 (2006), 1121–1136.

[Bolanowski et al. 88] S. J. Bolanowski, G. A. Gescheider, R. T. Verrillo, and C. M. Checkosky. "Four channels mediate the mechanical aspects of touch." *Journal of the Acoustical Society of America* 84:5 (1988), 1680–1694.

[Brown and Colgate 98] J. Michael Brown and J. Edward Colgate. "Minimum Mass for Haptic Display Simulations." In *Proceedings ASME International Mechanical Engineering Congress and Exhibition*, 61, 61, pp. 85–92. Anaheim, CA: ASME, 1998.

[Brown 95] J. Michael Brown. "A Theoretical and Experimental Investigation into the Factors Affecting the Z-Width of a Haptic Display." Master's thesis, Northwestern University, Evanston, IL, 1995.

[Colgate and Brown 94] J. Edward Colgate and J. Michael Brown. "Factors Affecting the Z-Width of a Haptic Display." In *IEEE International Conference on Robotics and Automation*, 4, 4, pp. 3205–3210. San Deigo, CA: IEEE, 1994.

[Colgate and Hogan 88] J. Edward Colgate and Neville Hogan. "Robust Control of Dynamically Interacting Systems." *International Journal of Control* 48:1 (1988), 65–88.

[Colgate and Schenkel 97] J. Edward Colgate and Gerd G. Schenkel. "Passivity of a Class of Sampled-Data Systems: Application to Haptic Interfaces." *Journal of Robotic Systems* 14:1 (1997), 37–47.

[Colgate et al. 93] J. Edward Colgate, Michael C. Stanley, and Gerd G. Schenkel. "Dynamic range of achievable impedances in force reflecting interfaces." In *Telemanipulator Technology and Space Telerobotics*, 2057, 2057, pp. 199–210. Baltimore, MD: SPIE, 1993.

[Colgate et al. 95] J. Edward Colgate, Michael C. Stanley, and J. Michael Brown. "Issues in the Haptic Display of Tool Use." In *IEEE/RSJ International Conference on Intelligent Robots and Systems*, 3, 3, pp. 140–145. Pittsburgh, PA: IEEE, 1995.

[Desoer and Vidyasagar 75] C.A. Desoer and M. Vidyasagar. *Feedback Systems: Input-Output Properties*. New York, USA: Academic Press, 1975.

[Diolaiti and Niemeyer 06] Nicola Diolaiti and Günter Niemeyer. "Wave Haptics: Providing Stiff Coupling to Virtual Environments." In *IEEE Symposium on Haptic Interfaces*, 4, 4, pp. 185–192. Alexandria, VA: IEEE, 2006.

[Diolaiti et al. 06] Nicola Diolaiti, Günter Niemeyer, Federico Barbagli, and J. Kenneth Salisbury. "Stability of Haptic Rendering: Discretization, Quantization, Time-Delay and Coulomb Effects." *IEEE Transactions on Robotics* 22 (2006), 256–268.

[Gillespie and Cutkosky 96] R. Brent Gillespie and Mark R. Cutkosky. "Stable User-Specific Haptic Rendering of the Virtual Wall." In *ASME International Mechanical Engineering Conference and Exposition, DSC*, 58, 58, pp. 397–406. Atlanta, GA: ASME, 1996.

[Gosline et al. 06] Andrew H. Gosline, Gianni Campion, and Vincent Hayward. "On the Use of Eddy Current Brakes as Tunable, Fast Turn-On Viscous Dampers for Haptic Rendering." In *Eurohaptics*, pp. 229–234. Paris, France, 2006.

[Hannaford et al. 01] Blake Hannaford, Jee-Hwan Ryu, and Yoon S. Kim. "3 - Stable Control of Haptics." In *Touch in Virtual Environments: Proceedings USC Workshop on Haptic Interfaces*, edited by Margret McLaughlin. Prentice Hall, 2001.

[Janabi-Sharifi et al. 00] Farrokh Janabi-Sharifi, Vincent Hayward, and Chung-Shin J. Chen. "Discrete-Time Adaptive Windowing for Velocity Estimation." *IEEE Transactions on Control Systems Technology* 8:6 (2000), 1003–1009.

[Karnopp et al. 00] Dean C. Karnopp, Donald L. Margolis, and Ronald C. Rosenberg. *System Dynamics: Modeling and Simulation of Mechatronic Systems*, Third edition. New York, USA: A Wiley-Interscience Publication, 2000.

[Kawai and Yoshikawa 02] Masayuki Kawai and Tsuneo Yoshikawa. "Haptic Display of Movable Virtual Object with Interface Device Capable of Continuous-Time Impedance Display by Analog Circuit." In *IEEE International Conference on Robotics and Automation*, pp. 229–234. Washington, DC: IEEE, 2002.

[Kawai and Yoshikawa 04] Masayuki Kawai and Tsuneo Yoshikawa. "Haptic Display with an Interface Device Capable of Continuous-Time Impedance Display Within a Sampling Period." *IEEE/ASME Transactions on Mechatronics* 9:1 (2004), 58–64.

[Kuchenbecker et al. 06] Katharine J. Kuchenbecker, Jonathan Fiene, and Günter Niemeyer. "Improving contact realism through event-based haptic feedback." *IEEE Transactions on Visualization and Computer Graphics* 12 (2006), 219–230.

[Lawrence et al. 00] Dale A. Lawrence, Lucy Y. Pao, Anne M. Dougherty, Mark A. Salada, and Yiannis Pavlou. "Rate-hardness: a new performance metric for haptic interfaces." *IEEE Transactions on Robotics and Automation* 16 (2000), 357–371.

[Mehling et al. 05] Joshua S. Mehling, J. Edward Colgate, and Michael A. Peshkin. "Increasing the Impedance Range of a Haptic Display by Adding Electrical Damping." In *IEEE First World Haptics Conference and Symposium*, pp. 257–262. Pisa, Italy: IEEE, 2005.

[Miller et al. 00] Brian E. Miller, J. Edward Colgate, and Randy A. Freeman. "Guaranteed Stability of Haptic Systems with Nonlinear Virtual Environments." *IEEE Transactions on Robotics and Automation* 16:6 (2000), 712–719.

[Miller et al. 04] Brian E. Miller, J. Edward Colgate, and Randy A. Freeman. "On the role of dissipation in haptic systems." *IEEE Transactions on Robotics* 20 (2004), 768–771.

[Okamura et al. 98] Allison M. Okamura, Jack T. Dennerlein, and Robert D. Howe. "Vibration Feedback Models for Virtual Environments." In *IEEE International Conference on Robotics and Automation*, 3, 3, pp. 2485–2490. Leuven, Belgium: IEEE, 1998.

[Okamura et al. 01] Allison M. Okamura, Mark R. Cutkosky, and Jack T. Dennerlein. "Improving Reality-Based Models for Vibration Feedback." *IEEE/ASME Transactions on Mechatronics* 6:3 (2001), 245–252.

[Ryu et al. 04] Jee-Hwan Ryu, Yoon S. Kim, and Blake Hannaford. "Sampled- and continuous-time passivity and stability of virtual environments." *IEEE Transactions on Robotics* 20:4 (2004), 772–776.

[Ryu et al. 05] Jee-Hwan Ryu, Carsten Preusche, Blake Hannaford, and Gerd Hirzinger. "Time-domain Passivity Control with Reference Energy Following." *IEEE Transactions on Control Systems Technology* 13:5 (2005), 737–742.

[Salcudean and Vlaar 97] S. E. Salcudean and T. D. Vlaar. "On the Emulation of Stiff Walls and Static Friction with a Magnetically Levitated Input-Output Device." *Transactions of the ASME: Journal of Dynamics, Measurement and Control* 119:1 (1997), 127–132.

[Stramigioli et al. 02] Stefano Stramigioli, Cristian Secchi, Arjan J. van der Schaft, and Cesare Fantuzzi. "A novel theory for sample data systems passivity." In *IEEE/RSJ International Conference on Intelligent Robots and Systems*, pp. 1936–1941. Lausanne, Switzerland: IEEE, 2002.

[Zilles and Salisbury 95] C. Zilles and K. Salisbury. "A Constraint-Based God Object Method for Haptic Display." In *IEEE/RSJ International*

Conference on Intelligent Robots and Systems, 3, 3, pp. 146–151. Pittsburgh, PA: IEEE, 1995.